Computer Methods and Programs in Biomedicine 241 (2023) 107744

Contents lists available at ScienceDirect

Computer Methods and Programs in Biomedicine

journal homepage: www.elsevier.com/locate/cmpb

The Cilialyzer – A freely available open-source software for the analysis of mucociliary activity in respiratory cells

Martin Schneiter [a,b,*], Stefan A. Tschanz [b], Anaïs Escher [c,d], Loretta Müller [c,d], Martin Frenz [a,*]

[a] Institute of Applied Physics, University of Bern, Sidlerstrasse 5, 3012 Bern, Switzerland
[b] Institute of Anatomy, University of Bern, Baltzerstrasse 2, 3012 Bern, Switzerland
[c] Department of Paediatrics, Inselspital Bern, University Hospital, University of Bern, 3010 Bern, Switzerland
[d] Department of BioMedical Research, University of Bern, 3008 Bern, Switzerland

ARTICLE INFO

Keywords:
High-speed video microscopy (HSVM)
Primary ciliary dyskinesia (PCD)
Ciliary beat frequency (CBF)
Mucociliary clearance (MCC)
Air-liquid interface (ALI)
Mucociliary activity

ABSTRACT

Background and Objective: Primary ciliary dyskinesia (PCD) is a rare genetic disorder causing a defective ciliary structure, which predominantly leads to an impaired mucociliary clearance and associated airway disease. As there is currently no single diagnostic gold standard test, PCD is diagnosed by a combination of several methods comprising genetic testing and the examination of the ciliary structure and function. Among the approved diagnostic methods, only high-speed video microscopy (HSVM) allows to directly observe the ciliary motion and therefore, to directly assess ciliary function. In the present work, we present our recently developed freely available open-source software – termed "Cilialyzer", which has been specifically designed to support and facilitate the analysis of the mucociliary activity in respiratory epithelial cells captured by high-speed video microscopy.

Methods: In its current state, the Cilialyzer software enables clinical PCD analysts to load, preprocess and replay recorded image sequences as well as videos with a feature-rich replaying module facilitating the commonly performed qualitative visual assessment of ciliary function (including the assessment of the ciliary beat pattern). The image processing methods made accessible through an intuitive user interface allow clinical specialists to comfortably compute the ciliary beating frequency (CBF), the activity map and the "frequency correlation length" – an observable getting newly introduced. Furthermore, the Cilialyzer contains a simple-to-use particle tracking interface to determine the mucociliary transport speed.

Results: Cilialyzer is fully written in the Python programming language and freely available under the terms of the MIT license. The proper functioning of the computational analysis methods constituting the Cilialyzer software is demonstrated by using simulated and representative sample data from clinical practice. Additionally, the software was used to analyze high-speed videos showing samples obtained from healthy controls and genetically confirmed PCD cases (DNAI1 and DNAH11 mutations) to show its clinical applicability.

Conclusions: Cilialyzer serves as a useful clinical tool for PCD analysts and provides new quantitative information awaiting to be clinically evaluated using cohorts of PCD. As Cilialyzer is freely available under the terms of a permissive open-source license, it serves as a ground frame for further development of computational methods aiming at the quantification and automation of the analysis of mucociliary activity captured by HSVM.

1. Introduction

The inner surface of our airways is lined by a mucous fluid film, which is permanently propelled into the direction of the throat. The propulsion of this airway surface liquid (ASL) is provided by the collectively coordinated oscillatory motion of a myriad of subjacent cilia. Inhaled particles get entrapped by the ASL layer and subsequently transported into the direction of the throat, where they finally get swallowed. Thereby, mucociliary clearance (MCC) constitutes our airway's primary defense mechanism by protecting our airways from inhaled toxic and infectious agents [1].

The importance of the proper functioning of motile cilia is particularly highlighted by its failure in primary ciliary dyskinesia (PCD), which is predominantly characterized by chronic airway infections.

* Corresponding authors.
E-mail addresses: martin.schneiter@unibe.ch (M. Schneiter), martin.frenz@unibe.ch (M. Frenz).

https://doi.org/10.1016/j.cmpb.2023.107744
Received 19 August 2022; Received in revised form 12 July 2023; Accepted 2 August 2023
Available online 10 August 2023

PCD is a genetic disorder with an autosomal recessive inheritance pattern and an estimated incidence of 1:7'500 to 1:20'000 [2,3]. Mutations in (at least) one of many genes coding for proteins involved in ciliary assembly lead to a defective ciliary structure exhibiting an impaired (or absent) ciliary motion, which in turn, is commonly thought to result in an insufficient (or absent) mucociliary clearance. The various PCD-causing genetic mutations are associated with different structural and functional defects resulting in different pathological patterns. This contributes to the challenges of diagnosis [4]. It has to be highlighted that the actual observable of interest – namely, the efficacy of the mucociliary airway clearance – is presently not directly accessible. This raises the challenging fundamental question of how to most adequately infer the efficacy of the actual mucociliary clearance and to reliably recognize an impairment of the latter.

Today, the efficacy of the actual mucociliary clearance function in PCD suspects is inferred by visually examining microscopic high-speed recordings, which merely show the ciliary motion on a few brushed nasal epithelial cells immersed in culture medium (e.g. see [5]). These conditions greatly differ from the native conditions, in which the air-exposed viscoelastic mucus layer gets propelled by the underlying collectively coordinated ciliary activity of large contiguous arrays of ciliated cells.

Due to the unavailability of easy-to-use fast software tools allowing for a convenient quantitative analysis, the conventional HSVM analysis currently mainly relies on the visual recognition of clearly discernible defects in the ciliary beating pattern (CBP). This requires extensive empirical experience, is time-consuming and is highly subjective. The CBF is the only quantitative observable being routinely determined in diagnostic centers. Even though the conventional HSVM approach is commonly considered as the most sensitive and specific test to identify PCD [6], its lack of standardization prevents its use as a confirmatory diagnostic test, or its inclusion in a diagnostic algorithm [7].

Among the currently approved diagnostic methods, however, the functional analysis performed by HSVM can be seen as the most direct method to diagnose PCD, as it allows to directly observe the mucociliary activity. Therefore, HSVM will continue to play an important role in PCD diagnostics as well as for the examination of the various functional phenotypes and the establishment of relations to the associated genotypes.

When examining the presently available body of literature, two main lines of research revolving around the development of techniques aiming towards a quantitative characterization of the high-speed recordings of ciliary activity become apparent. Motivation for both lines of research is to contribute to the standardization of the HSVM analysis.

In the first line of research, dedicated computational methods aiming at the quantitative, objective and automated detection of defects in the ciliary motion on detached and immersed respiratory epithelial cells are developed [8–18]. Those studies mainly focus on the quantitative and automated characterization of the ciliary motion pattern of individual cilia and therefore, at making the conventional HSVM approach observer-independent. However, from a wider perspective, the reliability of the conventionally performed HSVM approach is inherently limited, as detached ciliated cells being immersed in culture medium can only partly reflect the quality of the primary MCC mechanism. The MCC mechanism is an excellent example for a complex dynamical system with a local-to-global character, as the local fluid mechanical interactions of oscillating individual cilia are thought to generate the collective motion pattern, which eventually generates efficient mucociliary transport [19–21]. How the characteristic motion pattern of individual cilia is related to the collective ciliary motion pattern largely remains obscure. But, it can be presumed that small modulations in the individual ciliary motion pattern will amplify due to local fluid mechanical interactions and thus be more clearly reflected by the collective ciliary motion pattern [22]. This presumption is tightly connected to the second line of research, which aims to investigate and quantify the collective mucociliary phenomena in human respiratory re-differentiated cell cultures, which are grown and observed at the air-liquid interface (e.g. see [23–28]). From a physical point of view, this semi-artificial system matches the natural conditions more closely, as – in contrast to the medium-immersed brushed epithelial cells used in the classical clinical HSVM approach – it presents an air-exposed viscoelastic mucus layer [29].

In summary, both lines of research have brought up new useful image processing methods allowing for a quantitative characterization of mucociliary activity. However, in diagnostics and clinical research, it is often not possible to use those image analysis routines, as either they are not freely accessible, or not provided with an intuitive easy-to-use user interface. Therefore, we have developed the herein presented freely accessible highly user-oriented open-source software, termed 'Cilialyzer'. The Cilialyzer software is not only meant to serve as a clinical tool to support diagnostic analyses of ciliary activity, but also as a framework for the development of further computational methods for both above-mentioned lines of research.

2. Methods

2.1. Sample preparation & imaging

The Cilialyzer software was designed for the analysis of dynamic high-speed recordings showing different types of samples from the respiratory epithelium. Therefore, neither the details of the sample preparation nor of the imaging are crucial for the video processing methods presented in this work. The sample preparation and the imaging used to eventually record the herein shown high-speed videos have recently been reported in great detail [30,31]. Briefly, the image data shown here represent microscopic images showing the motion of cilia in three commonly used types of samples. Sample type I: medium-immersed human nasal epithelial cells, which were harvested by nasal brushings (see Fig. 1A). Sample type II: medium-immersed re-differentiated epithelial cells, which were scratched off from intact cultures of mucociliary epithelium grown at the air-liquid interface (ALI) (see Fig. 1B). Sample type III: intact cultures of mucociliary epithelium, which were grown as well as observed at the ALI (see Fig. 1C). Note that Fig. 1A–C represent single frames of the high-speed videos (Video S1–S3), which are provided as supplemental material.

Brushed nasal epithelial cells were cultured at the air-liquid interface using the PneumaCult media from Stemcells (described in detail in [30]). Briefly, cells were proliferated using the PneumaCult Expansion Plus medium, then seeded in 12-well transwells with a pore size of 0.4 μm and exposed to the air for differentiation after full confluence. The cells were fed with PneumaCult ALI medium for four weeks until they were fully differentiated and showed mucus production and beating cilia. The day before the measurements, fully differentiated cell cultures were washed with phosphate-buffered saline (PBS with magnesium and calcium) for 30 minutes at 37 °C to remove excess mucus and the media in the basolateral chamber was renewed.

After brushing or scratching, respectively, samples of type I and type II were brought into sealed chambers, which are built by a microscope slide, a 200 μm thick rubber spacer and a cover glass on top [30]. The suspensions of cells were imaged in bright field using an inverted transmitted light microscope (Olympus IX73). By using a bright field 40×-objective (Olympus UMPlan Fluorit, water immersion, NA 0.8, WD 3.3 mm) an area of approximately 55×40 μm^2 was imaged onto the CMOS chip of a digital high-speed camera (GS3-U3-32S4M-C, FLIR Integrated Imaging Solutions Inc., Canada). Samples of type III were kept in culture well plates during observation. As for this kind of observation, an objective with a longer working distance was needed (Olympus UPlan SemiApo, 10× phase contrast, NA 0.3, WD 10 mm), the field of view amounts to approximately 220×165 μm^2. For all three types of samples, the pixel resolution was set to 640×480 and ciliary activity was recorded at 300 frames per second over a time span of 2 seconds. All recordings shown in this work were taken at a temperature of 37 °C.

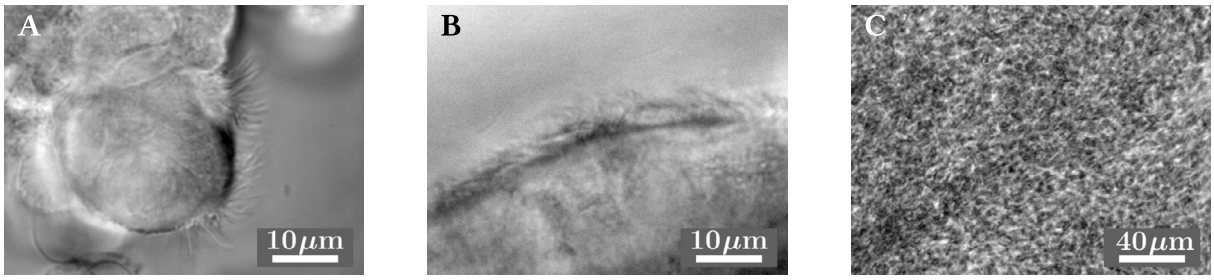

Fig. 1. The three depicted microscopic images represent single frames of three typical high-speed recordings showing the ciliary activity within sample type I - III. The distinguishing characteristics of the different sample types can be nicely seen. A: freshly brushed human nasal epithelial cells immersed in culture medium (sample type I). This sample type is mainly characterized by the availability of only small groups of cells consisting of few ciliated cells. B: medium-immersed re-differentiated epithelial cells, which were scratched off from intact cultures of mucociliary epithelium grown at the ALI. Overall, the sample quality (in terms of cell and cilia population as well as vitality) of sample type II is typically better than in samples of type I. C: intact cultures of mucociliary epithelium grown as well as observed at the ALI (sample type III). A large array of epithelial cells can be seen (basolateral view).

For more detailed information on the sample preparation, the imaging of sample type I–III and our diagnostic procedure please refer to [30] and [31].

Sample population

The exemplary sample data shown were derived from seven healthy controls and four PCD patients: 2× homozygous for DNAI1, 1× compound heterozygous for DNAH11 (referred in the following as DNAH11-1) and 1× homozygous for DNAH11 (referred in the following as DNAH11-2). Gender and age of all subjects can be found in Sec. S1. The study was approved by the ethics committees of the University Children's Hospital Bern and of the canton Bern, Switzerland (reference no. 2018-02155). Written informed consent was obtained from every participant or her/his legal guardian.

2.2. Video analysis procedure

In this section, the mathematical methods get introduced as well as illustrated by exemplary sample data from clinical practice. Please understand that care must be taken when interpreting the results provided by the software. For PCD specialists, we recommend to carefully read the present work and the enclosed manual, which contains more information on the practical use of the software.

Fig. 2 shows an overview of the video analysis procedure for all three sample types. Each processing step is explained in detail in the following sections.

2.2.1. Reading the data; matching the camera to the microscope

The Cilialyzer allows to import image sequences as well as videos in most common open image and video formats, respectively. Before reading in the data, the user has to specify the frames per second (FPS) and the pixel size[1] to be used for the analysis. These two parameters will specify the temporal and spatial resolution of the video to be analyzed.

Besides other important considerations to be made when choosing the components of a high-speed video microscope setting, it is particularly important to match the camera to the microscope. If no additional optics, such as a video coupler device is used, the spatial lateral resolution of a transmitted-light microscope is roughly given by Abbe's limit. The spatial resolution of the camera is roughly given by $2.3 \cdot \delta / m$, where δ represents the physical pixel size of the camera and m the magnification of the microscope. Consequently, in order to not reduce the optical resolution by the choice of the camera, the physical pixel size δ should ideally meet the following condition:

$$\delta \leq \frac{\lambda \cdot m}{4.6 \cdot \mathrm{NA}}\,, \tag{1}$$

where λ represents the wavelength of the light source and NA the objective's numerical aperture.

2.2.2. Preprocessing

As has been shown previously (e.g. see [8,9]), the high-speed recordings need to be adequately preprocessed before getting analyzed. In the following, we describe the available video-preprocessing steps, which mainly take care of the removal of disturbing movements and vibrations of the whole sample and the removal of the static background, emphasizing the actual signal of interest.

Image stabilization

Image stabilization, or image registration, designates the process of aligning consecutive images and represents a highly important preprocessing step. Depending on the sample, image stabilization serves for the removal of cell or tissue motion. Before stabilizing the image sequence, the user has the possibility to manually rotate as well as to select a region of interest (ROI).

In order to get rid of undesirable sample motions, and thus to stabilize the image sequences, Cilialyzer uses the Python package 'pyStackReg' [32] to align each image $\mathrm{I}[x,y,t]$ to the mean image $\langle \mathrm{I}[x,y,t] \rangle_t$, by performing a rigid body transform (translation and rotation). Note that $\langle \ldots \rangle_t$ denotes the average calculated along the time axis. Since each image is aligned to the same common reference image, the computation time could be significantly shortened by distributing the computation across N processes running in parallel (where N either designates the number of available CPU cores less 1, or the number of cores set by the user that may be used for image stabilization). In order to further shorten the computation time, the user can specify how many consecutive frames may be skipped during the stabilization process (0–3 frames). Skipped frames get then transformed in the exact same way as its predecessor.

After the image stabilization process, the image sequence needs to be slightly cropped, as the stabilization process adds invalid pixels at the margins.

Motion extraction

As has been shown e.g. in [8,9], the static background of an image sequence $\mathrm{I}[x,y,t]$ can be removed by subtracting the mean image:

$$\mathrm{I'}[x,y,t] = \mathrm{I}[x,y,t] - \langle \mathrm{I}[x,y,t] \rangle_t\,, \tag{2}$$

Note that the mean image subtraction, as denoted in Eq. (2), is equivalent to removing the zero-frequency contribution along the time axis (for each pixel separately).

[1] Please note that 'pixel size' refers to how many nanometers a pixel in each recorded image corresponds to in real units – and does not refer to the physical pixel size of the camera in use.

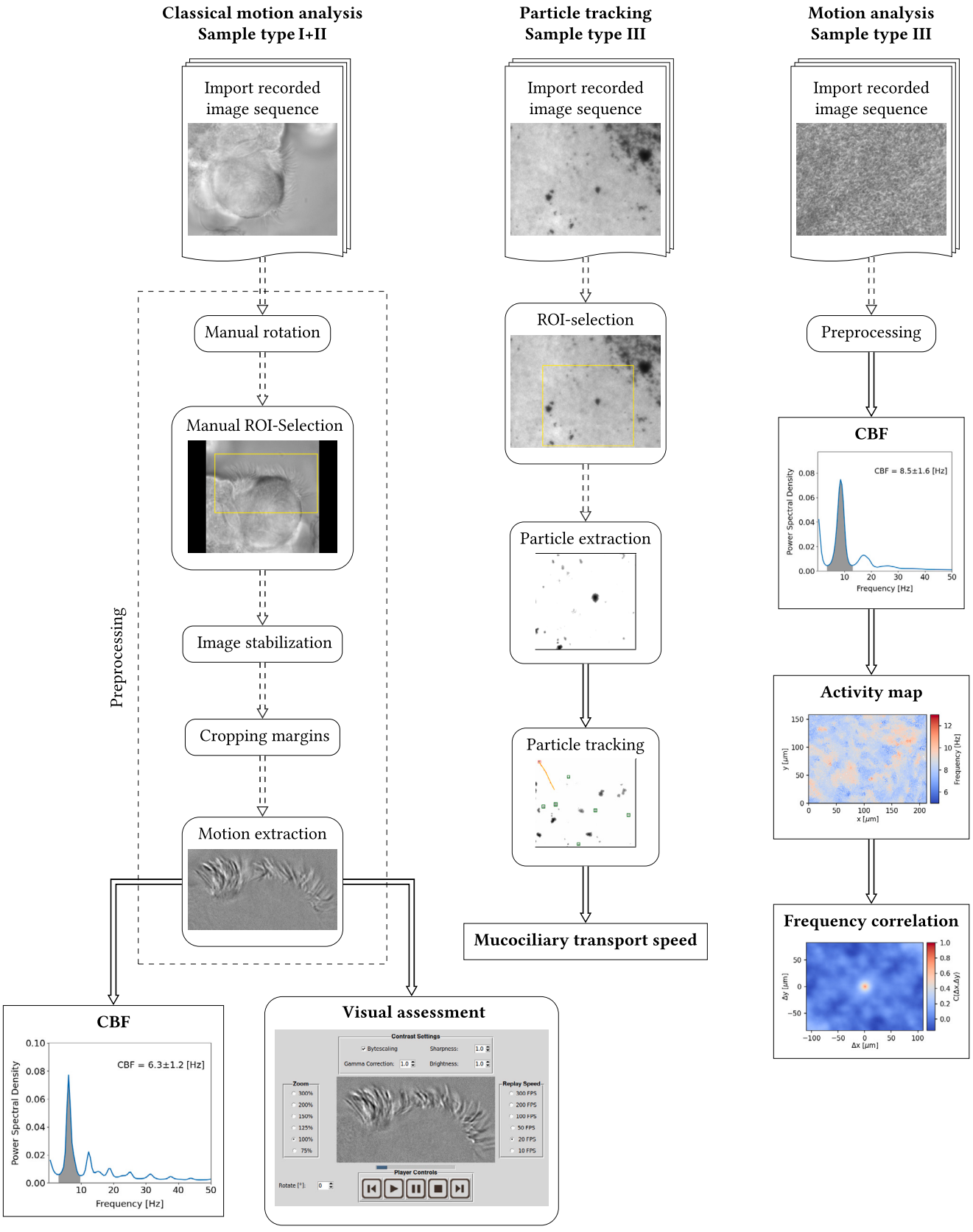

Fig. 2. Overview of the video analysis procedures for all three sample types.

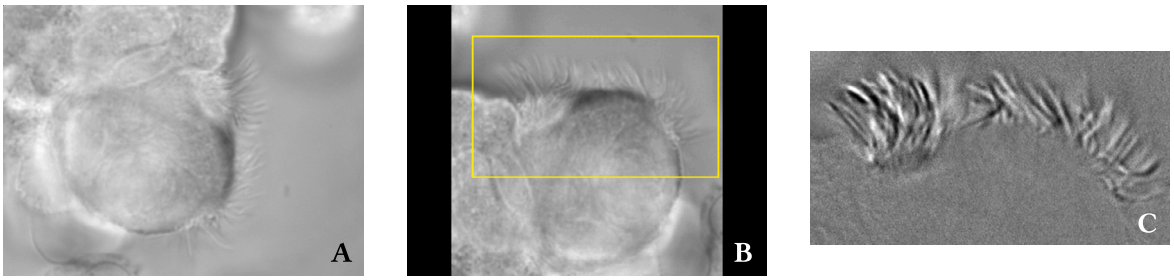

Fig. 3. A: snapshot of an original high-speed recording showing the motion of cilia on a few epithelial cells (sample type I). The cilia can just be recognized by eye. B: The yellow surround indicates the manually selected ROI, which can be chosen in the rotated image sequence. C: snapshot of the manually selected ROI after having performed the preprocessing. The cilia and their motion are now more clearly distinguished from the background.

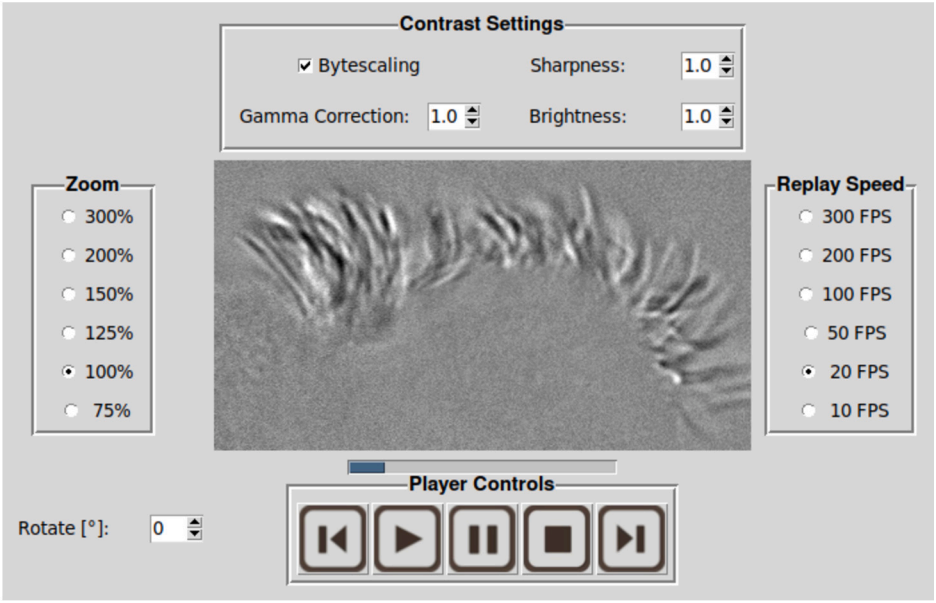

Fig. 4. Screenshot of Cilialyzer's replaying module. After having extracted the ciliary motion, which is to be investigated, clinical specialists can make use of the controls, which allow to adjust the playback speed, the zoom level and the contrast.

2.2.3. *Visual assessment*

The current clinical HSVM analysis procedure is primarily based on the visual recognition of abnormalities in the ciliary motion pattern (commonly referred to as the ciliary beat pattern). Therefore, the Cilialyzer software was also specifically developed to improve and facilitate the visual assessment of the activity.

Clinical specialists can make use of the just described preprocessing, by: rotating the video, selecting a ROI, stabilizing the video and finally extracting the ciliary motion as needed (see Fig. 3). The purpose of these preprocessing steps is to remove anything but the signal to be examined – i.e. the moving cilia. After having preprocessed the video, the Cilialyzer provides a replaying module (see Fig. 4), which allows PCD analysts to control the playback speed, the zoom level as well as to enhance the contrast as needed and is therefore perfectly suited for the common visual assessment of the ciliary beating pattern (e.g. see [30]).

2.2.4. *Computation of the ciliary beating frequency (CBF)*

The ciliary beating frequency (CBF) is determined from the average relative power spectral density (PSD), which represents the average over all relative PSDs derived from the intensity variations of all the pixels within a manually selected ROI (or within the whole field of view).

In more detail, the CBF is computed as follows. The intensity variation of a single pixel located at (x, y) can be considered as a time series $\mathrm{I}_{xy}(t)$. Generally, the PSD of an arbitrary time series $\mathrm{I}_{xy}(t)$ sampled at discrete times $t = 0, 1, ..., N_t - 1$ is defined as the absolute square of its corresponding Fourier amplitudes $\tilde{\mathrm{I}}_{xy}(f)$, which are computed by the discrete Fourier transform:

$$\tilde{\mathrm{I}}_{xy}(f) = \sum_{t=0}^{N_t-1} \mathrm{I}_{xy}(t) \cdot \exp\left(-2\pi i f t / N_t\right) \ , \tag{3}$$

where $f = 0, 1, ..., N_t - 1$ is a discrete array index representing the dimensionless frequency. The discrete Fourier transform (Eq. (3)) gets computed by using the highly efficient Fast Fourier transform (FFT) [33]. The PSD of a single pixel located at (x, y), denoted by $\mathrm{P}_{xy}(f)$, is given by the absolute square of its complex Fourier amplitudes: $\mathrm{P}_{xy}(f) = |\tilde{\mathrm{I}}_{xy}(f)|^2$. Furthermore, let $\hat{\mathrm{P}}_{xy}(f)$ be the relative (or normalized) PSD in the positive frequency range: $\hat{\mathrm{P}}_{xy}(f) = \left(\sum_{f\geq 0} \mathrm{P}_{xy}(f)\right)^{-1} \cdot \mathrm{P}_{xy}(f)$. Finally, in order to get insight into the frequency contributions within the manually selected ROI (or the whole field of view), comprising $N_x \cdot N_y$ pixels, the Cilialyzer eventually displays the average relative PSD, denoted as $\langle \hat{\mathrm{P}}_{xy}(f) \rangle_{xy}$, in the positive frequency range:

$$\langle \hat{\mathrm{P}}_{xy}(f) \rangle_{xy} = (N_x N_y)^{-1} \sum_{xy} \hat{\mathrm{P}}_{xy}(f). \tag{4}$$

Please note that the displayed average relative power spectral density gets slightly smoothed with a Gaussian kernel $\mathrm{G}_{\sigma=1}$, which can be denoted by the following convolution: $\langle \hat{\mathrm{P}}_{xy}(f) \rangle_{xy} * \mathrm{G}_{\sigma=1}$. Furthermore, the zero-frequency contribution gets omitted.

The CBF is finally determined as the weighted average (getting specified in the following) within the bandwidth $[f_1, f_2]$ belonging to the

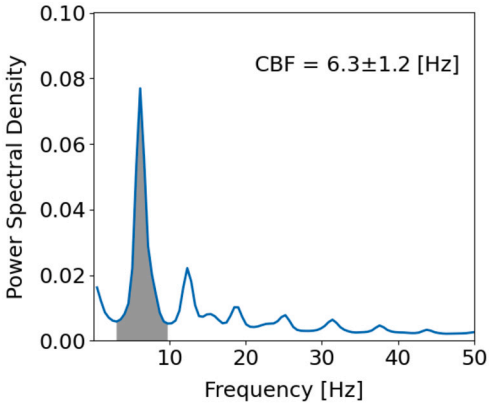

Fig. 5. Typical average relative PSD computed for the rectangular user-selection shown in Fig. 3B.

main peak, which is indicated by the gray shading in Fig. 5. Note that the series of peaks at integer multiples of the CBF represent higher harmonics, which indicate that the intensity variations are not purely harmonic. The calculation of the CBF requires two cut off frequencies f_1 and f_2, which represent the lower and upper limit of the main peak in the average relative PSD. Cilialyzer automatically suggests those two cut off frequencies (according to the procedure explained in Sec. S2). However, the user has also the possibility to manually adjust the bandwidth selection.

The array index f represents the dimensionless frequency, which can be transformed into its corresponding physical unit Hertz, denoted as $F(f)$, according to: $F(f) = f \cdot FPS/N_t$, where FPS denotes the frame rate (in [Hz]) at which the images have been recorded and N_t denotes the number of captured frames. The mean CBF, denoted as $\langle F \rangle$ and the peak width, which is measured by the weighted standard deviation σ_F, are then calculated according to:

$$\langle F \rangle = \left\{ \left(\sum_{f_i=f_1}^{f_2} w_{f_i} \right)^{-1} \sum_{f_i=f_1}^{f_2} w_{f_i} \cdot f_i \right\} \cdot \frac{FPS}{N_t} \qquad \sigma_F = \sqrt{\langle F^2 \rangle - \langle F \rangle^2}\,, \quad (5)$$

where the weights w_{f_i} are given by the average relative PSD: $w_{f_i} = \langle \hat{\mathrm{P}}_{xy}(f_i) \rangle_{xy}$. Finally, $\langle F^2 \rangle$ in Eq. (5) was calculated analogously to $\langle F \rangle$: $\langle F^2 \rangle = \left\{ \left(\sum_{f_i=f_1}^{f_2} w_{f_i} \right)^{-1} \sum_{f_i=f_1}^{f_2} w_{f_i} \cdot f_i^2 \right\} \cdot \frac{FPS}{N_t}$.

2.2.5. Activity map

The activity map provides information on how the CBF is spatially distributed and can thus be seen as a position-resolved CBF map. The computation of the activity map follows the principles, which have previously been presented [34]. Note that an alternative algorithm allowing to robustly determine the activity map has very recently been presented in [28].

Recall that the pixel-specific relative power spectral density (PSD) is denoted as $\hat{\mathrm{P}}_{xy}(f)$. Usually, only a part of the field of view displays ciliary activity. Therefore, in order to discriminate between pixels exhibiting a reasonable PSD from invalid pixels, we make use of the following simple condition. On the basis of the average relative PSD, i.e. $\langle \hat{\mathrm{P}}_{xy}(f) \rangle_{xy}$ defined in Eq. (4), we can define the total power P contributed by all the frequencies found inside the bandwidth of the main peak: $P = \sum_{f_i=f_1}^{f_2} \langle \hat{\mathrm{P}}_{xy}(f_i) \rangle_{xy}$. Furthermore, let P_{xy} be the pixel-specific total power contributed in the bandwidth of the main peak, i.e. $P_{xy} = \sum_{f_i=f_1}^{f_2} \hat{\mathrm{P}}_{xy}(f)$. Finally, a pixel located at (x, y) is marked as invalid (NaN), if: $P_{xy}/P < \Theta$, where Θ represents a threshold value, which can be adjusted manually. The exact choice of Θ is not crucial and to some degree arbitrary, as its choice affects the result for the frequency correlation length only very slightly. Its optimal choice will depend on the recordings (sample type, noise level etc.). Θ will therefore needed to be tuned empirically. However, for most settings the optimal value will roughly lie between 0 and 0.3. For valid pixels, on the other hand, a location-resolved CBF is ascribed, which is computed according to Eq. (5) by replacing the average relative PSD $\langle \hat{\mathrm{P}}_{xy}(f_i) \rangle_{xy}$ with the pixel-specific PSD $\hat{\mathrm{P}}_{xy}(f)$.

2.2.6. Frequency correlation

The 'frequency correlation', denoted by ξ, refers to the correlation length in the spatial autocorrelation of the activity map and constitutes another feature of the Cilialyzer. The spatial autocorrelation of the activity map gets computed by exploiting the Wiener-Khinchin theorem, which states that the correlation function and the power spectrum are a pair of Fourier transforms. The inverse Fourier transform of the spatial power spectrum therefore yields the autocorrelation function. As the computation in the Cilialyzer takes the zero-padding as well as missing values into account (i.e. pixels showing an invalid power spectral density), the computation of the spatial autocorrelation of the activity map is not trivial. The interested reader is therefore referred to Sec. S4, where the computational details are outlined.

In simple terms, the frequency correlation ξ can be understood as the average distance over which the CBF roughly remains preserved. Another interpretation concerns ξ^2, which can be seen as the average patch size over which the frequency roughly remains preserved. Those patches can clearly be recognized by eye in the activity map provided in Fig. 6.

2.2.7. Mucociliary transport speed (particle tracking)

Especially in samples of type III, mucociliary transport represents a potentially insightful observable providing rather direct information on the efficacy of the mucociliary clearance mechanism. In order to adequately track the movement of the mucus layer, it is usually necessary to use some kind of tracers. Please note that particle suspensions – even though frequently used – are not well suited for the investigation of mucociliary transport, as droplets applied on the outermost mucus layer change the physical properties of the air-liquid interface and might even induce transport phenomena, which are not related to the underlying ciliary propulsion mechanism. Therefore, we recommend to blow a tiny amount of lightweight dry puff ball spores (from calvatia excipuliformis) onto the mucus surface, as was done previously [31,34–37].

The Cilialyzer's particle tracking module consists of a simple-to-use interface, which allows the user to extract and select the particles to be tracked. Since the tracers are small point-like structures, they can optionally be extracted by subtracting a basically blurred copy (Lee-filtering followed by Gaussian filtering) from the original image sequence. A subsequent thresholding removes some residual background. The particle tracking is based on a local extremum tracker within a manually adjustable window size. This yields noisy particle trajectories, which need to be adequately fitted, in order to correctly determine the curve length. As has been observed previously in vitro [24,27], mucociliary epithelium grown at the ALI in circularly confined culture vessels typically exhibits circular mucociliary transport. This means that particles can run along circular, spiral or quasi-linear trajectories. Therefore, the noisy particle traces are first slightly smoothed and subsequently fitted by a univariate spline, whose curve length is finally used to determine the mucociliary transport speed. This procedure is highly robust and can cope with arbitrary particle trajectories.

3. Results

3.1. Software

The herein presented computational methods constitute the Cilialyzer, which is a freely available open-source software. It is fully written in the Python programming language [38] and distributed under the terms of the MIT license with the additional request to include a citation

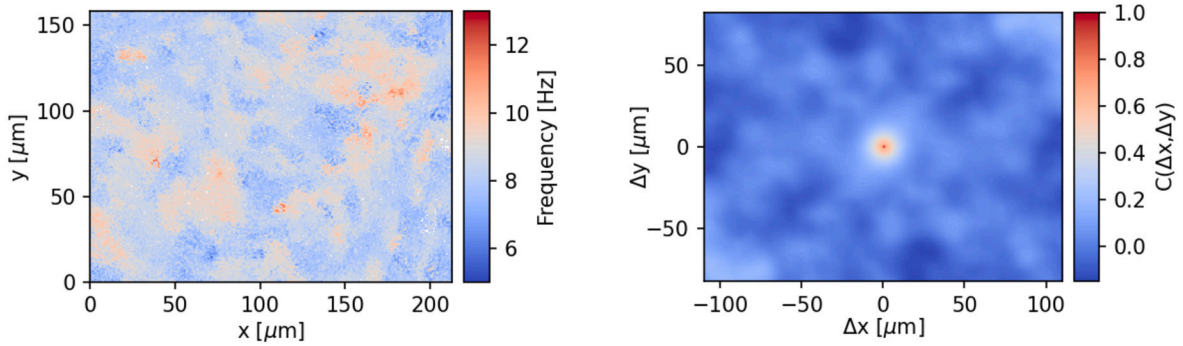

Fig. 6. Left: activity map showing the spatial distribution of the CBF in a re-differentiated cell culture grown at the air-liquid interface (sample type III) generated from video S3. Right: frequency correlation i.e. the spatial autocorrelation of the activity map shown on the left. The size of the central peak can be seen as a measure for the average patch size recognizable in the activity map.

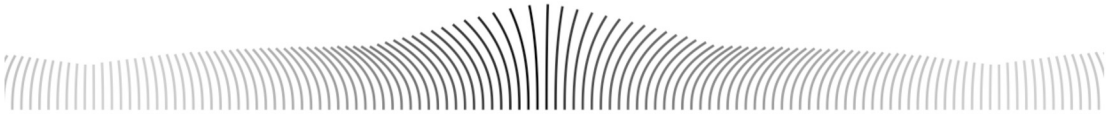

Fig. 7. Snapshot of the simulated ciliary array used to validate the computation of the CBF.

of the present manuscript. The source code, tutorials as well as compiled releases are provided at Github: https://github.com/msdev87/Cilialyzer. Readers who are mainly interested in downloading and using the application are referred to: https://msdev87.github.io/Cilialyzer. However, users are kindly asked to carefully read the work at hand and the enclosed manual – and to ensure that the results displayed in Cilialyzer can be correctly interpreted.

3.2. Preprocessing

On the one hand, an adequate preprocessing improves the visual assessment, as the image stabilization and the subsequent subtraction of the static background highlights the moving cilia to the observer. On the other hand, distorting movements of the whole sample must be eliminated in order to ensure the correctness of the objective quantitative analysis (see the example of a compromised CBF computation in the subsequent section). The enclosed videos S4–S6 are meant to illustrate the power of the presently available preprocessing and represent preprocessed versions of videos S1–S3.

3.3. Validation of the CBF-computation

It has been shown previously (e.g. see [39,40]) that the CBF computed by means of the power spectral density of the pixel's intensity variations corresponds well to the manually determined CBF, which is performed by progressing the high-speed videos frame by frame in order to visually count the ciliary oscillation period. For reassurance, we have shown that the computed CBF matches the manually determined CBF very well (see Sec. S3 in the supplementary material). Additionally, similar to the approach chosen in [41], the correctness of the output frequency can be shown by recovering a predefined input frequency. For this purpose, we have simulated a metachronally coordinated array of cilia, which is shown in Fig. 7.

See also video S7, which provides an example of the ciliary array oscillating at 10 Hertz. This array of cilia was used to generate 20 videos, in which the cilia oscillate with a predefined input oscillation frequency ranging from 1 to 20 Hertz. Fig. 8 shows that the input frequency (simulated CBF) corresponds exactly to the output frequency (measured CBF) determined by the Cilialyzer.

3.3.1. Importance of the image stabilization

The important role of the image stabilization is best illustrated with an example from clinical practice. When considering the high-speed recording provided by video S8, which shows a freshly excised group of nasal epithelial cells (sample type I), it can be seen that the ciliary motion is superposed by a quasi-periodic movement of the whole group of cells. Video S9 shows a stabilized and cropped version of video S8. Fig. 9A shows the CBF computation based on the non-preprocessed video S8, whereas Fig. 9B shows the CBF computation based on the preprocessed video S9. In Fig. 9A, it can be nicely seen that without any preprocessing the average power spectrum gets completely compromised by the superposed motion of the whole group of cells. The actual CBF-peak is hardly recognizable and the selection of the CBF-bandwidth becomes a guessing game. Whereas, the average power spectral density we are actually looking for and which corresponds to the ciliary motion can be recovered by performing the preprocessing, as can be seen in Fig. 9B.

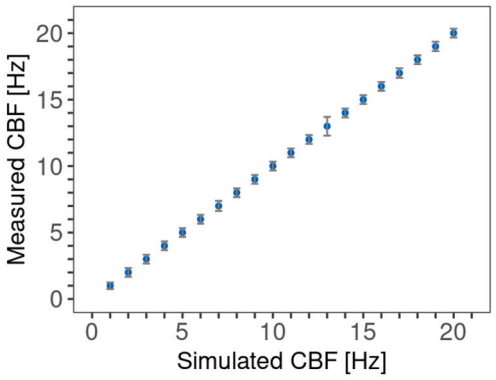

Fig. 8. For the functional testing of the CBF-computation, an array of cilia was simulated to oscillate in the range from 1 to 20 Hertz, which corresponds to the input frequency shown on the x-axis. The graph shows that the CBF as determined by the Cilialyzer (shown on the y-axis) exactly matches the simulated input frequency.

3.4. Spatial distribution of the CBF

Similar to the validation of the CBF-computation presented in the previous section, we verified the proper functioning of the computation of the activity map and the frequency correlation length with simulated data.

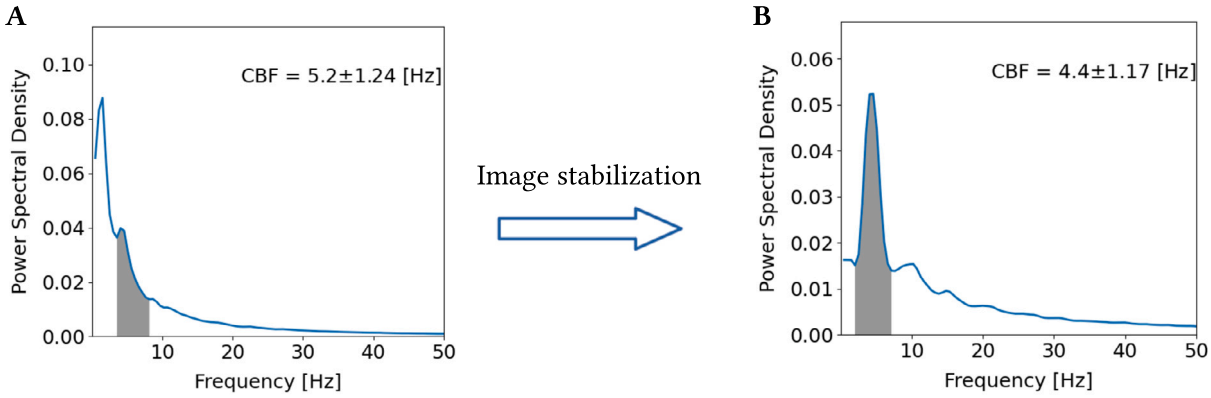

Fig. 9. A: average power spectral density based on the non-preprocessed video S8: the actual CBF-peak is hardly recognizable and the selection of the CBF-bandwidth becomes a guessing game. B: After performing the preprocessing, the average power spectral density, which actually corresponds to the ciliary motion becomes apparent.

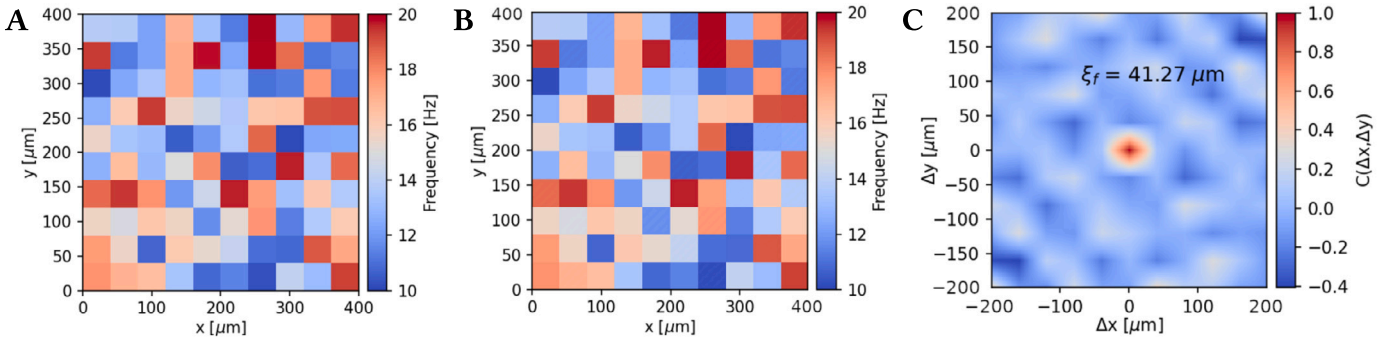

Fig. 10. For the functional testing of the computation of the activity map and the frequency correlation length, we simulated harmonic plane waves with a clustered frequency distribution. The quadratic clusters are clearly visible in panel A and panel B, which show the simulated (ground truth; with frequencies ranging from 10 to 20 Hz) activity map and the computed activity map inferred by the Cilialyzer algorithm. C: The frequency correlation length ξ_f provides a measure for the distance over which the frequency remains roughly preserved.

In order to illustrate the proper functioning of the methods, the analysis of a single example video used for functional testing is shown in the following. The simulated image sequence is provided in the supplementary material (see video S10). The artificially generated video shows the propagation of harmonic plane waves. While the harmonic plane waves were all generated with the same wavelength, the frequency was set in a semi-random manner in the range from 10 to 20 Hertz. The field of view was divided into 10×10 square clusters, each having a size of 40×40 pixels. While the frequency was set constant for all pixels within each cluster, the cluster frequency was chosen randomly. The simulated clustered frequency distribution is shown in Fig. 10A, whereas panel B shows the corresponding activity map computed by the Cilialyzer. Fig. 10C finally shows the spatial autocorrelation function of the activity map and displays the frequency correlation length ξ_f. In the Cilialyzer we assumed that one pixel corresponds to 1 μm^2 – representing in principle an arbitrarily defined scale. Considering that the frequency correlation is intended to represent an observable, which provides rather relative[2] than absolute information about the distance over which the CBF roughly remains preserved, the absolute value of roughly 41 pixels (compare with Fig. 10C) is very close to the actual cluster size, which was chosen to be 40 pixels.

3.5. Sample analyses

In this section we present sample data determined with Cilialyzer for samples of type II and type III. While the healthy individuals differ between the two sample types (with one exception, HC-2), the PCD data shown for sample type II was derived from the same cell culture (as well as the same person) as the PCD data shown for sample type III. In total, data derived from 2×4 healthy volunteers, 2 DNAI1 and 2 DNAH11 PCD patients is shown. Cilialyzer was used to process 6–10 videos of each person.

3.5.1. Sample type 2

Fig. 11A shows the boxplots illustrating the distribution of the CBF within each individual person, as determined in recordings of medium-immersed nasal epithelial cells scratched off from intact ALI cell cultures by using Cilialyzer. The person-specific median CBF values range from 4.0–10.6 Hz. In all samples derived from the two DNAI1 patients, the cilia were completely immotile/static. Accordingly, the CBF in these samples was 0 Hz. Finally, both DNAH11 patients exhibited clearly hyperfrequent median ciliary beating frequencies of 18.6 and 20.8 Hz.

3.5.2. Sample type 3

In videos of samples of type III, i.e. intact whole ALI cultures kept in closed culture plates, Cilialyzer allows to characterize the mucociliary activity in terms of the CBF, the frequency correlation length and the mucociliary transport speed.

CBF: Fig. 11B shows the distribution of the CBF within each individual person. As can be seen, the healthy median values show a low variability and they all range only from 7.9 to 8.7 Hz. Despite the extensive use of the preprocessing methods, only noise could be extracted in all PCD samples. Accordingly, the CBF was assumed to be 0 Hz.

Frequency correlation length: The value for the frequency correlation length could be determined for all healthy samples. Considering its rel-

[2] As compared to recordings captured according to the same experimental procedure.

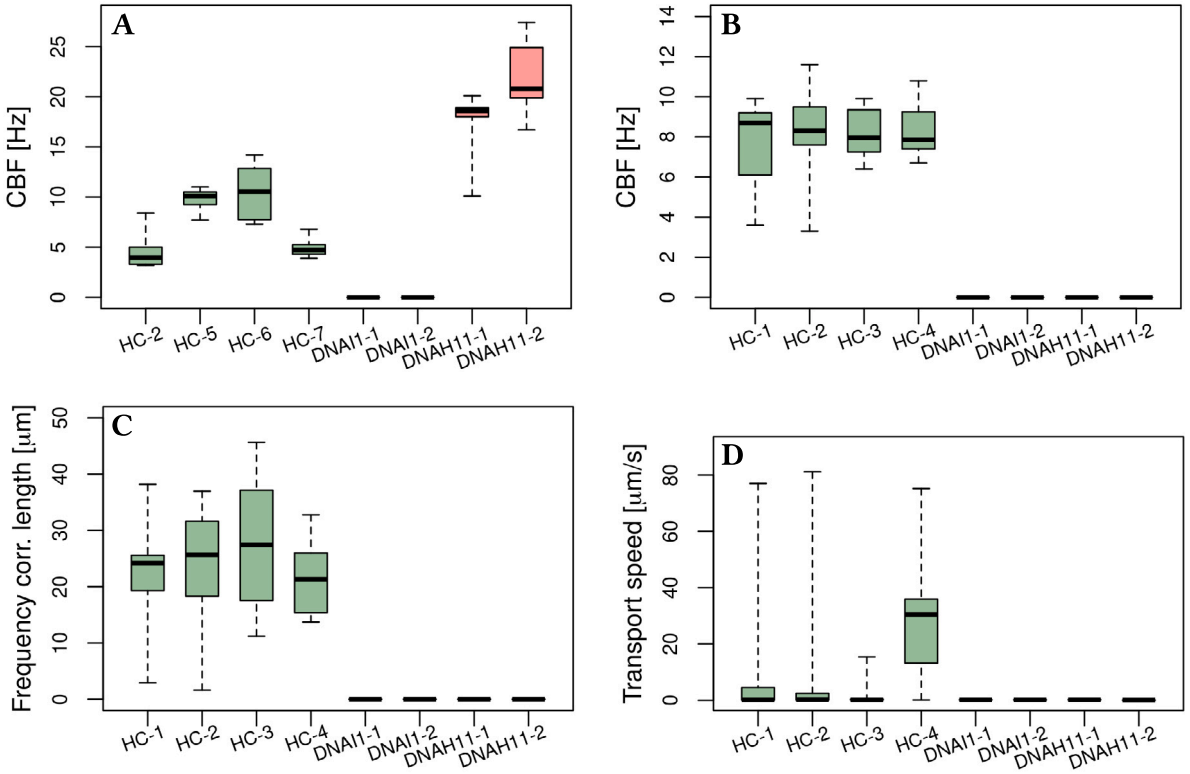

Fig. 11. Whiskers indicate the full range of values. A: person-specific CBF distributions as derived from samples of type II. B–D: person-specific distribution of determined values in samples of type III for the CBF (B), the frequency correlation length (C) and the mucociliary transport speed (D).

atively complex computation and meaning, the values for the frequency correlation length exhibit a remarkably low variability (see Fig. 11C). As only noise could be extracted in videos collected from all four PCD patients, the frequency correlation length was close to 0 µm in each video.

Mucociliary transport speed: As can clearly be seen in Fig. 11D, the mucociliary transport speed, as measured at randomly chosen sites, shows a right-skewed distribution within each healthy individual. This is due to the fact that at the time the measurement was taken, there was no mucus located at the chosen site; and we could clearly observe that no measurable particle transport takes place at sites showing no (or too little) mucus. Therefore, the maximum values for the mucociliary transport speed are more relevant here. In healthy samples, the maximum transport speed ranged from 15.4 to 81.1 µm/s. In all samples derived from the PCD patients, all measured transport speed values were lower than 0.4 µm/s. As the camera pixel size was 0.344 µm, the window size was chosen to measure 20×20 pixels and each recording time corresponds to 10 s, the measured transport speed would in any case have to amount to at least 0.5 µm/s to be considered a significant transport. Therefore, no significant transport was measured in all PCD samples.

4. Discussion

This work presents the current version of the freely available Cilialyzer software, which we specifically developed to improve and facilitate the analysis of ciliary function captured by HSVM. We envision the Cilialyzer software not only as a clinical tool for the analysis of mucociliary activity, but also as a ground frame for the future development of an even more comprehensive consensus-based application, which allows clinical specialists as well as biomedical researchers to automatically and quantitatively detect impaired mucociliary activity. The functional testing, i.e. the proper implementation of the accessible computational methods, is demonstrated by using either simulated data or examples from clinical practice. The Cilialyzer software is therefore ready for comprehensive clinical validation studies.

In comparison to applications, which were developed for the analysis of ciliary function in HSVM recordings and were recently made publicly available (e.g. see [39,40,42]), the Cilialyzer software offers many advantages. The present version can be easily customized and extended, as Python is well suited for rapid prototyping. Users do not need a license or a virtual machine to run the software, and for users working on Microsoft Windows, there is the possibility to download a compiled binary release, which is available on GitHub: https://github.com/msdev87/Cilialyzer. The Cilialyzer represents the most comprehensive application serving for the analysis of mucociliary activity in HSVM recordings. From a clinical point of view, the Cilialyzer stands out not only because of its ease of use, but also because of the many pre-processing and replaying options it offers. After loading an image sequence or a video (in almost any common format), the Cilialyzer particularly offers the possibility to easily rotate the sequence, select a ROI, remove undesirable tissue motion, remove the static background, enhance the contrast, zoom-in and set the playback speed. The enclosed videos S4-S6 and S9, which represent pre-processed versions of the videos S1-S3 and S8, respectively, are intended to provide an idea of the available pre-processing options. In the pre-processed videos, the ciliary motions are clearly emphasized, which – since the Cilialyzer does not yet comprise computational methods allowing for a quantitative assessment of the ciliary beat pattern – supports and facilitates the common visual assessment of the ciliary beating pattern. The visual assessment of the CBP is a subtle task, based on which experienced PCD analysts can achieve a high accuracy in identifying aberrations to the healthy CBP (e.g. see [6]). In recordings captured by HSVM, the ciliary motion is often superposed by motions of the whole specimen or by motions of the cells (see video S8). As shown in Sec. 3.3.1, such videos can be stabilized (see video S9) allowing for a reliable CBF-determination.
For the above-mentioned reasons, the Cilialyzer is ideally suited for the current clinical assessment of ciliary function in medium-immersed epithelial airway cells (sample type I and II), which primarily consists of

the CBF-computation and the visual assessment of the ciliary motion pattern (e.g. see [6,30]).

Thanks to the availability of affordable high-performance computers and the ongoing development of new dedicated image processing techniques, it will soon be possible to retrieve considerably more quantitative information from the high-speed recordings. We are strongly convinced that this will significantly enhance the reliability of future HSVM outcomes in PCD diagnostics.

From a wider perspective, detached ciliated cells being immersed in culture medium, i.e. sample type I and II, can only partly reflect the quality of the primary mucociliary clearance mechanism, which is the actual variable of interest to be judged. We therefore believe that specimens of sample type III, i.e. intact re-differentiated respiratory cell cultures, which are grown as well as observed at the air-liquid interface, harbor the greatest potential in terms of the information content about the primary mucociliary clearance. The following reasons support this presumption. 1) In contrast to brushed respiratory epithelial cells suspended in culture medium, cell cultures grown at the ALI match the natural physical conditions more closely, as they present an air-exposed mucus layer. 2) The actual variable of interest, namely the mucociliary transport speed, can be measured directly after applying lightweight dry puff ball spores, which have been used previously [31,34–37] and are ideally suited to track the movement of the mucus layer. Please note that the speed of suspended microbeads was shown to exhibit an essentially parabolic decrease with an increasing distance to the ciliary tips in samples of type I and II [18]. The current Cilialyzer version does not yet offer the possibility to measure the distance to the ciliary tips and can therefore only be used for transport speed measurements in samples of type III. 3) Compared to the recordings of medium-immersed brushed epithelial cells, the recordings of ciliary activity in intact ALI cultures are much more homogeneous – in terms of their occurrence and orientation to the optical axis – facilitating the use and development of quantitative image processing methods. This is reflected in the applicability of the frequency correlation length, which was tested and does not represent a meaningful observable for sample type I and II, as they appear in too different forms making comparability between determined values for the frequency correlation length impossible. 4) The ciliary activity of a much greater number of cells can be recorded. Since we know that the CBF can vary significantly between individual cells – or between groups of cells, averaging over a much greater number of cells is expected to significantly increase the diagnostic value of the CBF. This can clearly be seen when comparing the distribution of the CBF for sample type II and III (see Sec. 3.5). To our knowledge, the diagnostic significance of the CBF, when determined from samples of type III remains to be properly studied. The interested reader is also referred to Sec. S5 in the supplementary material, where the spatial variance of the CBF is illustrated for all three sample types. 5) Finally, mucociliary transport represents a collective phenomenon and it can be presumed that small modulations in the individual ciliary motion pattern will amplify due to local fluid mechanical interactions and thus be more clearly reflected by the collective ciliary motion pattern [22].

Therefore, we are confident that the HSVM analysis will run in the direction of this newly emerging type of genuine functional PCD diagnostics and have started to develop mathematical methods allowing for the quantitative (and automated) characterization of the collective mucociliary activity in ALI cultures. Currently, the Cilialyzer offers to use the preprocessing, replaying, CBF computation and the generation of the activity map for all types of samples. Whereas, the frequency correlation and the particle tracking deliver meaningful values only for samples of type III. From a classical point of view, the greatest potential for improvement of the Cilialyzer as a diagnostic tool for PCD, most probably lies in the quantification of the CBP. However, according to the above reasoning, samples of type III harbor a lot of information, which has not yet been made quantitatively accessible – especially concerning the collective ciliary beat pattern, which we are currently trying to quantify in terms of space-time correlations. Since the values determined within healthy samples (see Fig. 11) delivered consistent results, the frequency correlation length serves as a first observable characterizing the collective ciliary beating. The significance of the observables for PCD diagnostics, especially as determined in recordings of sample type III, remains to be properly studied. By using the Cilialyzer, the CBF, the mucociliary transport speed as well as the frequency correlation length can now be determined and need to be clinically validated.

Future incorporations of further methods, will allow for a more precise characterization of the collective ciliary motion in ALI cultures, which in turn, will allow for a more sensitive identification of impairments of the collective mucociliary activity. To clinical PCD analysts, we therefore would like to propose to use the Cilialyzer software to fully explore the diagnostic value of the CBF, the mucociliary transport speed and the frequency correlation length determined in sample type III.

Finally, we are looking forward to a broad user and developer community and hope that with the help of the Cilialyzer software, many of the mentioned open questions will be addressed in clinical studies.

Ethical approval

The study was approved by the ethics committees of the University Children's Hospital Bern and canton Bern, Switzerland (reference no. 2018-02155). Written informed consent was obtained from every participant or her/his legal guardian.

CRediT authorship contribution statement

Martin Schneiter: Conceptualization; Data curation; Formal analysis; Investigation; Methodology; Software; Validation; Visualization; Writing – original draft preparation; Writing – review & editing. **Stefan A. Tschanz:** Conceptualization; Funding acquisition; Investigation; Methodology; Project Administration; Resources; Supervision; Validation; Writing – original draft preparation; Writing – review & editing. **Anaïs Escher**: Investigation; Writing – review & editing. **Loretta Müller:** Conceptualization; Funding acquisition; Investigation; Methodology; Project administration; Resources; Writing – review & editing. **Martin Frenz:** Conceptualization; Funding acquisition; Investigation; Methodology; Project administration; Supervision; Writing – review & editing.

Declaration of competing interest

We confirm that this manuscript has not been published elsewhere and is not under consideration in any other journal. All authors have approved the manuscript and they agree with its submission to Computer Methods and Programs in Biomedicine. All the authors confirm that they do not have any conflict of interest.

Acknowledgements

This work was co-funded by the Swiss Lung Foundation. Part of the microscopic work was performed on equipment of the Microscopy Imaging center (MIC) of the University of Bern. Study authors participate in the BEAT-PCD clinical research collaboration (CRC), supported by the European Respiratory Society. Our PCD-UNIBE diagnostic center participates in the European Reference Network (ERN) Lung PCD core as a supporting member. Finally, we would like to express our sincere thanks to Jaroslav Rička, who acted as a main source of inspiration for this work.

Appendix A. Supplementary material

Supplementary material related to this article can be found online at https://doi.org/10.1016/j.cmpb.2023.107744.

References

[1] Janna C. Nawroth, Anne M. Van Der Does, Amy Ryan, Eva Kanso, Multiscale mechanics of mucociliary clearance in the lung, Philos. Trans. R. Soc. Lond. B, Biol. Sci. 375 (1792) (2020) 1–8.

[2] Michael R. Knowles, Leigh Anne Daniels, Stephanie D. Davis, Maimoona A. Zariwala, Margaret W. Leigh, Primary ciliary dyskinesia: recent advances in diagnostics, genetics, and characterization of clinical disease, Am. J. Respir. Crit. Care Med. 188 (8) (2013) 913–922.

[3] William B. Hannah, Bryce A. Seifert, Rebecca Truty, Maimoona A. Zariwala, Kristen Ameel, Yi Zhao, Keith Nykamp, Benjamin Gaston, The global prevalence and ethnic heterogeneity of primary ciliary dyskinesia gene variants: a genetic database analysis, Lancet Respir. Med. 10 (5) (2022) 459–468.

[4] J.S. Lucas, A. Barbato, S.A. Collins, M. Goutaki, L. Behan, D. Caudri, S. Dell, E. Eber, E. Escudier, R.A. Hirst, C. Hogg, M. Jorissen, P. Latzin, M. Legendre, M.W. Leigh, F. Midulla, K.G. Nielsen, H. Omran, J.F. Papon, P. Pohunek, B. Redfern, D. Rigau, B. Rindlisbacher, F. Santamaria, A. Shoemark, D. Snijders, T. Tonia, A. Titieni, W.T. Walker, C. Werner, A. Bush, C.E. Kuehni, European Respiratory Society guidelines for the diagnosis of primary ciliary dyskinesia, Eur. Respir. J. 49 (1) (2017) 1601090.

[5] Céline Kempeneers, Claire Seaton, Bernardo Garcia Espinosa, Mark A. Chilvers, Ciliary functional analysis: beating a path towards standardization, Pediatr. Pulmonol. 54 (10) (2019) 1627–1638.

[6] Bruna Rubbo, Amelia Shoemark, Claire L. Jackson, Robert Hirst, James Thompson, Joseph Hayes, Emily Frost, Fiona Copeland, Claire Hogg, Christopher O'Callaghan, Isabel Reading, Jane S. Lucas, Accuracy of high-speed video analysis to diagnose primary ciliary dyskinesia, Chest 155 (5) (2019) 1008–1017.

[7] Noemie Bricmont, Mihaela Alexandru, Bruno Louis, Jean-François Papon, Céline Kempeneers, Ciliary videomicroscopy: a long beat from the European Respiratory Society guidelines to the recognition as a confirmatory test for primary ciliary dyskinesia, Diagnostics 11 (9) (2021).

[8] E. Puybareau, H. Talbot, G. Pelle, B. Louis, J.F. Papon, A. Coste, L. Najman, A regionalized automated measurement of ciliary beating frequency, in: 2015 IEEE 12th International Symposium on Biomedical Imaging (ISBI), IEEE, New York, NY, USA, 2015, pp. 528–531.

[9] Élodie Puybareau, Hugues Talbot, E. Bequignon, B. Louis, G. Pelle, A. Coste, Laurent Najman, Automating the measurement of physiological parameters: a case study in the image analysis of cilia motion, in: 2016 IEEE International Conference on Image Processing, Phoenix, AZ, USA, 2016, pp. 1240–1244.

[10] Meekail Zain, Sonia Rao, Nathan Safir, Quinn Wyner, Isabella Humphrey, Alex Eldridge, Chenxiao Li, BahaaEddin AlAila, Shannon Quinn, Towards an unsupervised spatiotemporal representation of cilia video using a modular generative pipeline, in: Proceedings of the 19th Python in Science Conference, number Scipy, 2020, pp. 166–175.

[11] Shannon P. Quinn, Maliha J. Zahid, John R. Durkin, Richard J. Francis, Cecilia W. Lo, S. Chakra Chennubhotla, Automated identification of abnormal respiratory ciliary motion in nasal biopsies, Sci. Transl. Med. 7 (299) (2015) 299ra124.

[12] Shannon Quinn, Richard Francis, Cecilia Lo, Chakra Chennubhotla, Novel use of differential image velocity invariants to categorize ciliary motion defects, in: Proceedings of the 2011 Biomedical Sciences and Engineering Conference: Image Informatics and Analytics in Biomedicine, BSEC 2011, IEEE, 2011, pp. 10–13.

[13] Maurizio Chioccioli, Luigi Feriani, Quynh Nguyen, Jurij Kotar, Sharon D. Dell, Vito Mennella, Israel Amirav, Pietro Cicuta, Quantitative high-speed video profiling discriminates between DNAH11 and HYDIN variants of primary ciliary dyskinesia, Am. J. Respir. Crit. Care Med. 199 (11) (2019) 1436–1438.

[14] Woojae Kim, Tae Hwa Han, Hyun Jun Kim, Man Young Park, Ku Sang Kim, Rae Woong Park, An automated measurement of ciliary beating frequency using a combined optical flow and peak detection, Healthc. Inform. Res. 17 (2) (2011) 111–119.

[15] Eduardo Parrilla, Miguel Armengot, Manuel Mata, José Manuel Sánchez-Vílchez, Julio Cortijo, José L. Hueso, Jaime Riera, David Moratal, Primary ciliary dyskinesia assessment by means of optical flow analysis of phase-contrast microscopy images, Comput. Med. Imaging Graph. 38 (3) (2014) 163–170.

[16] O. Meste, F. Brau, A. Guyon, Robust estimation of the motile cilia beating frequency, Med. Biol. Eng. Comput. 53 (10) (2015) 1025–1035.

[17] Jean-François Papon, Laurence Bassinet, Gwenaëlle Cariou-Patron, Francoise Zerah-Lancner, Anne Marie Vojtek, Sylvain Blanchon, Bruno Crestani, Serge Amselem, Andre Coste, Bruno Housset, Estelle Escudier, Bruno Louis, Quantitative analysis of ciliary beating in primary ciliary dyskinesia: a pilot study, Orphanet J. Rare Dis. 7 (2012) 1–11.

[18] Mathieu Bottier, Sylvain Blanchon, Gabriel Pelle, Emilie Bequignon, Daniel Isabey, André Coste, Estelle Escudier, James B. Grotberg, Jean-François Papon, Marcel Filoche, Bruno Louis, A new index for characterizing micro-bead motion in a flow induced by ciliary beating: part I, experimental analysis, PLoS Comput. Biol. 13 (2017) 1–19.

[19] Martin Schneiter, Jaroslav Ricka, Martin Frenz, Self-organization of self-clearing beating patterns in an array of locally interacting ciliated cells formulated as an adaptive Boolean network, in: Theory in Biosciences, 2019.

[20] Douglas R. Brumley, Kirsty Y. Wan, Marco Polin, Raymond E. Goldstein, Flagellar synchronization through direct hydrodynamic interactions, eLife 3 (e02750) (2014).

[21] J. Elgeti, G. Gompper, Emergence of metachronal waves in cilia arrays, Proc. Natl. Acad. Sci. USA 110 (12) (2013) 4470–4475.

[22] Pietro Cicuta, The use of biophysical approaches to understand ciliary beating, Biochem. Soc. Trans. 48 (1) (2020) 221–229.

[23] Luigi Feriani, Maya Juenet, Cedar J. Fowler, Nicolas Bruot, Maurizio Chioccioli, Steven M. Holland, Clare E. Bryant, Pietro Cicuta, Assessing the collective dynamics of motile cilia in cultures of human airway cells by multiscale DDM, Biophys. J. 113 (1) (2017) 109–119.

[24] Mustapha Kamel Khelloufi, Etienne Loiseau, Marc Jaeger, Nicolas Molinari, Pascal Chanez, Delphine Gras, Annie Viallat, Spatiotemporal organization of cilia drives multiscale mucus swirls in model human bronchial epithelium, Sci. Rep. 8 (2018) 2447.

[25] P.R. Sears, C.W. Davis, M. Chua, J.K. Sheehan, Mucociliary interactions and mucus dynamics in ciliated human bronchial epithelial cell cultures, Am. J. Physiol., Lung Cell. Mol. Physiol. 301 (2) (2011) L181–L186.

[26] Patrick R. Sears, Kristin Thompson, Michael R. Knowles, C. William Davis, Human airway ciliary dynamics, Am. J. Physiol., Lung Cell. Mol. Physiol. 304 (3) (2013) 170–183.

[27] Patrick R. Sears, Wei-Ning Yin, Lawrence E. Ostrowski, Continuous mucociliary transport by primary human airway epithelial cells in vitro, Am. J. Physiol., Lung Cell. Mol. Physiol. 309 (2015) L99–L108.

[28] Fradique Ricardo, Erika Causa, Clara Delahousse, Jurij Kotar, Laetitia Pinte, Ludovic Vallier, Marta Vila-Gonzalez, Pietro Cicuta, Assessing motile cilia coverage and beat frequency in mammalian in-vitro cell culture tissues, bioRxiv, preprint, https://doi.org/10.1101/2023.03.22.533861, 2023.

[29] Myriam Jory, Karim Bellouma, Christophe Blanc, Laura Casanellas, Aurélie Petit, Paul Reynaud, Charlotte Vernisse, Isabelle Vachier, Arnaud Bourdin, Gladys Massiera, Mucus microrheology measured on human bronchial epithelium culture, Front. Phys. 7 (FEB 2019) 1–12.

[30] Loretta Müller, Sibel T. Savas, Stefan A. Tschanz, Andrea Stokes, Anaïs Escher, Mirjam Nussbaumer, Marina Bullo, Claudia E. Kuehni, Sylvain Blanchon, Andreas Jung, Nicolas Regamey, Beat Haenni, Martin Schneiter, Jonas Ingold, Elisabeth Kieninger, A comprehensive approach for the diagnosis of primary ciliary dyskinesia — experiences from the first 100 patients of the PCD-UNIBE diagnostic center, Diagnostics 11 (9) (2021) 1540.

[31] Anaïs Escher, Elisabeth Kieninger, Susan De Groof, Sibel T. Savas, Martin Schneiter, Stefan A. Tschanz, Martin Frenz, Philipp Latzin, Carmen Casaulta, Loretta Müller, In vitro effect of combined hypertonic saline and salbutamol on ciliary beating frequency and mucociliary transport in human nasal epithelial cells of healthy volunteers and patients with Cystic Fibrosis, J. Aerosol Med. Pulm. Drug Deliv. 36 (4) (2023) 171–180, https://doi.org/10.1089/jamp.2022.0026.

[32] Philippe Thévenaz, Urs E. Ruttimann, Michael Unser, A pyramid approach to subpixel registration based on intensity, IEEE Trans. Image Process. 7 (1) (1998) 27–41.

[33] James W. Cooley, John W. Tukey, An algorithm for the machine calculation of complex Fourier series, Math. Comput. 19 (90) (1965) 297–301.

[34] M. Ryser, A. Burn, T. Wessel, M. Frenz, J. Rička, Functional imaging of mucociliary phenomena: high-speed digital reflection contrast microscopy, Eur. Biophys. J. 37 (1) (2007) 35–54.

[35] F. Wyss, M. Schneiter, U. Hetzel, S. Keller, M. Frenz, J. Ricka, J.-M. Hatt, Investigation of the tracheal mucociliary clearance in snakes with and without boid inclusion body disease and lung pathology, J. Zoo Wildl. Med. 49 (1) (mar 2018) 223–226.

[36] Martin Schneiter, Sebastian Halm, Adolfo Odriozola, Helga Mogel, Jaroslav Rička, Michael H. Stoffel, Benoît Zuber, Martin Frenz, Stefan A. Tschanz, Multi-scale alignment of respiratory cilia and its relation to mucociliary function, J. Struct. Biol. 213 (1) (2021).

[37] Andreas Burn, Martin Schneiter, Manuel Ryser, Peter Gehr, Jaroslav Rička, Martin Frenz, A quantitative interspecies comparison of the respiratory mucociliary clearance mechanism, Eur. Biophys. J. 0123456789 (2022).

[38] Guido Van Rossum, Fred L. Drake, Python 3 Reference Manual, CreateSpace, Scotts Valley, CA, 2009.

[39] Pedro Sampaio, Mónica Ferro da Silva, Inês Vale, Mónica Roxo-Rosa, Andreia Pinto, Carolina Constant, Luisa Pereira, Carla M. Quintão, Susana S. Lopes, CiliarMove: new software for evaluating ciliary beat frequency helps find novel mutations by a Portuguese multidisciplinary team on primary ciliary dyskinesia, ERJ Open Res. 7 (1) (2021) 00792.

[40] Claire M. Smith, Jana Djakow, Robert C. Free, Petr Djakow, Rana Lonnen, Gwyneth Williams, Petr Pohunek, Robert A. Hirst, Andrew J. Easton, Peter W. Andrew, Christopher O'Callaghan. CiliaFA, A research tool for automated, high-throughput measurement of ciliary beat frequency using freely available software, Cilia 1 (2012) 1–7.

[41] Vito Renò, Mauro Sciancalepore, Giovanni Dimauro, Rosalia Maglietta, Michele Cassano, Matteo Gelardi, A novel approach for the automatic estimation of the ciliated cell beating frequency, Electronics (Switz.) 9 (6) (2020) 1–15.

[42] Joseph H. Sisson, J.A. Stoner, B.A. Ammons, T.A. Wyatt, All-digital image capture and whole-field analysis of ciliary beat frequency, J. Microsc. 211 (2) (2003) 103–111.